ANSWERS TO REFEREE#1

1) I appreciate the improvements and additions made to the manuscript. The structure was improved according to the editor's recommendation. Although very long and difficult to understand sentences were partially shortened, there are still relatively many language-related mistakes (e.g. the use of respectively on P8LL8) that could be corrected to improve readability. Please do not report significant results when not supported by the statistical analysis (P1LL26; also, no uncertainty of the slope estimates are provided here which could help the readers to form an opinion themselves). Similar issues had been criticized in the first version of the manuscript.

ANSWER: Slopes estimates and simulations are reported along their estimated errors (in the form of error bars in Figure 9a).

2) Furthermore, in that paragraph (P1LL26), the description of potential outside air influences and the comparison with slopes inferred using temperatures for a local weather station remains somewhat confusing and seem somewhat in reverse, with overall unclear implications. I think the authors could structure their thoughts more clearly here.

ANSWER: The authors think to the contrary that the text now explains the phenomenon well. As proposed by the editor, the following sentence was added at the end of the paragraph:
"This also highlights the particular experimental conditions in the laboratory, where other sources of water vapor (e.g., by opening the laboratory door) might have influenced the isotope compositions of the air."

3) Abstract: Although the additional information is worth reporting, the abstract may be shortened.

ANSWER: the abstract was substantially shortened (~5 lines were removed)

4) P4L28: Consider consistent use of SI units as suggested by the editor, also later in the manuscript.

ANSWER: this is now the case in the revised manuscript.

5) P4L29: Please consider defining „o.d." for a non-technical audience.

ANSWER: "o.d" and "i.d" are now "outside diameter" "inside diameter" in the revised manuscript.

6) P7L16: I suggest modifying the section title since the reference is not a proper reference and also unusual in a title.

ANSWER: "Craig and Gordon model" was erased from the title

7) P8LL8: Please correct the use of respectively.

ANSWER: The authors rewrote the section 2.7 omitting the term "resp.".

8) P13L14: Since the wind velocities are not the subject of study, consider putting it differently, i.e. specific wind velocities may have caused the observed differences.

ANSWER: In an evaporation study, the aerodynamic conditions in the "atmosphere" are crucial; therefore wind velocity profiles are important. In addition, the authors do not understand what the reviewer means by "specific wind velocity".

9) P16L12: Uncertainty values should not be set just arbitrarily; please provide a (brief) justification for the choice of values.

ANSWER: Indeed. The text was modified to:

"Standard errors for the parameters θ_{res} and θ_{sat} were set to 0.01 m3 m-3 (i.e., comparable to the soil water content probes' precision)"

1

ANSWERS TO REFEREE#2

3

4   1) The authors have answered to my questions and I do not want to argue with that.
5   But more importantly I appreciate very much the new section about testing the Craig
6   and Gordon model. This is exactly needed and it is these kind of questions that can
7   be addressed with the new method. The results are indeed puzzling and I would
8   have loved to see a possible explanation, if possible. The authors have unfortunately
9   never explained their definition of rh. And the explanation that eps_k should depend
10 on rh_EF-rh looks odd to me. rh should be e_a/e_EF with e_EF=rh_EF*esat(T_EF)
11 and e_a the vapour pressure of ambient air. Because of the Kelvin relationship and
12 as written in the manuscript, rh_EF is often taken as one. T_EF is changing over the
13 course of the experiment. Taking ambient rh would explain, for example, the rising
14 slope in Fig. 9a.

15

16 *ANSWER: ε_K does not depend on rh, but the* kinetic effect *is, as defined by*
17 *Equations 4a and b in the precedent manuscript. The kinetic effect evaluates both*
18 *impact of the water vapor potential gradient (rhEF-rha) and resistance of the air layer*
19 *opposed to water vapor flow (i.e., expressed through ε_K). In addition, variations of*
20 *T_EF are taken into account: it is the normalized rh_a that is being computed (4.3*
21 *PP14LL15)*

22

23 2) It is there that I would have loved to see a bit more explanations. rh_EF is just one,
24 and in my opinion an unlikely one. But then, the experimental results seem unlikely
25 as well. Would have been great to see a bit more other formulations of n or eps_k
26 besides Mathieu and Bariac such as the formulations in the first SiSPAT_iso paper
27 (Braud et al., J of Hydrol. 309, 277-300, 2005).

28

29 *ANSWER: Yes that would have been great! Unfortunately, we did not measure a*
30 *wind distribution profile to use the formulation of Merlivat and Coantic (1975) based*
31 *on the evaporation model of Brutsaert (1982). The other formulations (Melayah et al.,*
32 *1996 and Barnes and Allison, 1983) give α_K constant over time (n is constant in*
33 *these cases), therefore won't be able to explain a change of evaporation line slope*
34 *value through change of n.*

35

36 3) This would have sensitized the authors to the sloppy formulations they are using
37 when talking about diffusion, boundary layer and the like. For example, the
38 resistance to molecular diffusion is not dependent on the n-th power of diffusivity
39 ratio.

40

41 *ANSWER: However, this is exactly what Mathieu and Bariac (1996) say, reporting*
42 *Merlivat and Coantic (1975): "Assuming that the turbulent transport is*
43 *nonfractionating and that the molecular diffusion resistances r_M and r*_M are*
44 *proportional to the nth power of the diffusivities d_v and d*_v …".*

Nevertheless, this was reformulated in 2.7 following the terminology of Gat et al. (1971).

4) The diffusivity ratio gives directly the kinetic fractionation factor of molecular diffusion (n=1). n=2/3 is taken for boundary layer resistance. Turbulent transfer should have no fractionation at all, i.e. n=0. But there is always a boundary layer even over free water surfaces, so n=0.5 is an effective n.

Also the term boundary layer over the evaporating front is misleading. If the evaporative front is in the soil, then there is the soil matrix above the evaporative front, which most people would not have called a boundary layer but rather a layer of molecular resistance. Above the soil then comes the atmospheric boundary layer.

ANSWER: Indeed, this term is no longer used in that way in the current manuscript. Thank you.

5) The data is in my opinion not a test of Craig and Gordon but rather (of the formulation) of the kinetic fractionation factor. Might be different point of view.

ANSWER: This is right, this is now reformulated in the abstract as a test of the formulation of isotope kinetic effects and section 4.3 title is now "Isotope kinetic effects during soil evaporation"

6) So I would ask the authors to provide explanations about rh, e.g. by plotting it also in Fig. 9b; revisit their wording and explanations about diffusion, boundary layer and the like; and perhaps also include some other formulations for eps_k to find some reasoning behind the unexpected results.

ANSWER: See answers to comments 1)-4). In 4.3 is now the following § added:
"In a fourth scenario, the ratio of turbulent diffusion resistance to molecular diffusion resistance is no more negligible, leading to n' values ranging between 0 and n (Merlivat and Jouzel, 1979). This last scenario was however not verifiable. In any case, only decreasing kinetic effects could provide a better model-to-data fit. Note that the formulation of kinetic enrichments proposed by Merlivat and Coantic (1975) and based on the evaporation model of Brutsaert (1982) was not tested due to lack of appropriate data (i.e., unknown wind distribution profile over the soil column). The formulations of Mélayah et al. (1996) (n = 0) and Barnes and Allison (1983) (n = 1) were also not tested as they give kinetic enrichments constant over time and cannot explain a change of SEv value through change of n."

Long-term and high frequency non-destructive monitoring of water stable isotope profiles in an evaporating soil column

Y. Rothfuss[1], S. Merz[1], J. Vanderborght[1], N. Hermes[1], A. Weuthen[1], A. Pohlmeier[1], H. Vereecken[1] and N. Brüggemann[1]

[1]{Forschungszentrum Jülich GmbH, Institute of Bio- and Geosciences, Agrosphere Institute (IBG-3), Leo-Brandt-Straße, D-52425 Jülich, Germany}

Correspondence to: Y. Rothfuss (y.rothfuss@fz-juelich.de)

Abstract

The stable isotope compositions of soil water (δ^2H and δ^{18}O) carry important information about the prevailing soil hydrological conditions and for constraining ecosystem water budgets. However, they are highly dynamic, especially during and after precipitation events. ~~The classical method of determining soil water δ^2H and δ^{18}O at different depths, i.e., soil sampling and cryogenic extraction of the soil water, followed by isotope-ratio mass spectrometer analysis is destructive and laborious with limited temporal resolution. In this study, we present an application of~~ In this study, we present an application of a method based on gas-permeable tubing and isotope-specific infrared laser absorption spectroscopy for *in situ* determination of δ^2H and δ^{18}O. We conducted a laboratory experiment ~~with an acrylic glass column filled with medium~~ where a sand ~~equipped with gas-permeable tubing at eight different soil depths. The soil~~ column was initially saturated ~~from the bottom~~, exposed to evaporation for a period of 290 days, and finally rewatered. Soil water vapor δ^2H and δ^{18}O were measured daily~~, sequentially for~~ at each ~~depth.~~ of eight available depths. Soil liquid water δ^2H and δ^{18}O were inferred from ~~the isotopic values~~ those of the vapor assuming thermodynamic equilibrium between liquid and vapor phases in the soil. The experimental setup allowed following the evolution of ~~typical exponential-shaped~~ soil water δ^2H and δ^{18}O profiles with ~~unprecedentedly high~~ a daily temporal resolution. As the soil dried, we could also show for the first time the increasing influence of the isotopically depleted ambient water

1 vapor on the isotopically enriched liquid water close to the soil surface (i.e., atmospheric

2 invasion). Rewatering at the end of the experiment led to instantaneous resetting of the stable

3 isotope profiles, which could be closely followed with the new method.

4 From simple soil δ^2H and δ^{18}O gradients calculations, we showed that the gathered data

5 allowed to determinate the depth of the Evaporation Front (EF) and how it receded into the

6 soil overtime. It was inferred that after 290 days under the prevailing ~~laboratory air~~

7 ~~temperature, moisture, and aerodynamic~~experimental conditions, ~~and given the specific~~

8 ~~hydraulic properties of the sand,~~ the EF had moved down to an approximate depth of –0.06 m.

9 Finally, data was used to calculate evaporation lines' slopes and test the

10 ~~expression~~formulation for ~~the slope of evaporation lines proposed by Gat (1971) and based on~~

11 ~~the model of Craig and Gordon (1965).~~isotope kinetic effects. A very good agreement was

12 found between measured and simulated values (Nash and Sutcliffe Efficiency - NSE = 0.92)

13 during the first half of the experiment, i.e., until the EF reached a depth of –0.04 m. From this

14 point, calculated kinetic effects associated with the transport of isotopologues in the soil

15 surface air layer above the EF provided slopes lower than observed. Finally, values of isotope

16 kinetic effects that provided the best model-to-data fit (NSE > 0.9) were obtained from

17 inverse modelling, highlighting uncertainties associated with the determinations of isotope

18 kinetic fractionation and soil relative humidity at the EF.

19

20 1 Introduction

21 Stable isotopologues of water, namely ^{1}H^{2}H^{16}O and ^{1}H$_2$^{18}O are powerful tools used in a wide

22 range of research disciplines at different and complementary temporal and spatial scales. They

23 provide ways of assessing the origin of water vapor (e.g., Craig, 1961; Liu et al., 2010),

24 solving water balances of lakes (Jasechko et al., 2013) and studying groundwater recharge

25 (Blasch and Bryson, 2007; Peng et al., 2014). Analysis of the isotope compositions (δ^2H and

26 δ^{18}O) of soil surface and leaf waters allows for partitioning evapotranspiration into

27 evaporation and transpiration (e.g., Dubbert et al., 2013; Hu et al., 2014; Rothfuss et al., 2012;

28 Yepez et al., 2005).

29 Moreover, from soil water δ^2H and δ^{18}O profiles, it is also possible to derive quantitative

30 information, such as soil evaporation flux, locate evaporation fronts, and root water uptake

31 depths (Rothfuss et al., 2010; Wang et al., 2010). Zimmermann et al. (1967) and later Barnes

32 and Allison (1983, 1984) and Barnes and Walker (1989) first analytically described soil

1 $^1H^2H^{16}O$ and $^1H_2^{18}O$ movement at steady / non-steady state and in isothermal/ non-isothermal

2 soil profiles. Between precipitation events, the soil water δ^2H and $\delta^{18}O$ profiles depend on

3 flux boundary conditions, i.e., fractionating evaporation and non-fractionating capillary rise as

4 well as on soil properties (e.g., soil tortuosity). In a saturated soil, the isotope excess at the

5 surface due to evaporation diffuses back downwards, leading to typical and well documented

6 exponential-shaped δ^2H and $\delta^{18}O$ profiles. For an unsaturated soil, assuming in a first

7 approximation that isotope movement occurs in the vapor phase above the soil "evaporation

8 front" (EF) and strictly in the liquid phase below it, the maximal δ^2H and $\delta^{18}O$ values are no

9 longer observed at the surface but at the depth of EF. Above the EF, in the so-called "vapor

10 region", according to Fick's law, soil water δ^2H and $\delta^{18}O$ decrease towards the depleted

11 ambient atmosphere water vapor δ^2H and $\delta^{18}O$. Braud et al. (2005), Haverd and Cuntz (2010),

12 Rothfuss et al. (2012), Singleton et al. (2004), and Sutanto et al. (2012) implemented the

13 description of the transport of $^1H^2H^{16}O$ and $^1H_2^{18}O$ in physically based soil-vegetation-

14 atmosphere transfer (SVAT) models (HYDRUS 1D, SiSPAT-Isotope, Soil-Litter iso,

15 TOUGHREACT). In these models, movement of soil $^1H^2H^{16}O$ and $^1H_2^{18}O$ occur in both

16 phases below and above the EF, and heat and water transports are properly coupled.

17 However, these tools suffer from the comparison with other "traditional" methods developed

18 to observe and derive soil water state and transport. In contrast with soil water content and

19 tension measured by, e.g., time-domain reflectometry and tensiometry, isotope compositions

20 of soil water are determined either following destructive sampling or non-destructively but

21 with poor spatial and temporal resolution (i.e., with section cups in combination with

22 lysimeters for soil water tension higher than −600 hPa, e.g., Goldsmith et al., 2011, Litaor,

23 1988). This greatly limits their informative value. Only since recently, non-destructive

24 methodologies based on gas-permeable membrane and laser spectroscopy can be found in the

25 literature (Rothfuss et al., 2013; Herbstritt et al., 2012; Volkmann and Weiler, 2014, Gaj et

26 al., 2015).

27 The central objective of this study was to demonstrate that a direct application of the method

28 of Rothfuss et al. (2013) to a soil column would allow monitoring soil water δ^2H and $\delta^{18}O$

29 profiles in the laboratory with high temporal resolution and over a long time period. We will

30 demonstrate that the obtained isotope data can be used to locate the evaporation front as it

31 recedes into the soil during the experiment. Finally, data will be also used to test the

1   expression proposed by Gat (1971) and based on the Craig and Gordon (1965) of evaporation

2   lines' slopes.

3

4   **2   Material and methods**

5   **2.1   Isotopic analyses**

6   Isotopic analysis of liquid water and water vapor was performed using a cavity ring-down

7   spectrometer (L1102-i, Picarro, Inc., Santa Clara, CA, USA), calibrated against the

8   international primary water isotope standards V-SMOW2, GISP, and SLAP by liquid water

9   injection into the vaporizer of the analyzer. Primary and working standards' isotope

10   compositions were measured at 17,000 ppmv water vapor mixing ratio (number of replicates

11   = 4, number of injections per replicate = 8). Mean values and standard deviations were

12   calculated omitting the first three values of the first replicate to account for a potential

13   memory effect of the laser spectrometer. The laser spectrometer's dependence on water vapor

14   mixing ratio was also investigated according to the method of Schmidt et al. (2010).

15   Hydrogen and oxygen isotope ratios of water are expressed in per mil (‰) on the

16   international "delta" scale as defined by Gonfiantini (1978) and referred to as δ^2H and δ^{18}O,

17   respectively.

18   **2.2   Soil column and measurements**

19   The experiment was conducted in a 0.0057 m^3 acrylic glass column (0.11 m ~~i.d.,~~<u>inside</u>

20   <u>diameter,</u> 0.60 m height, Fig. 1a). The bottom of the column consisted of a porous glass plate

21   (10 ~~µm~~<u>10^{-6} m</u> < pore size diameter < 16 ~~µm~~<u>10^{-6} m</u> (4th class), Robu® GmbH, Hattert,

22   Germany) connected to a two-way manual valve (VHK2-01S-06F, SMC Pneumatik GmbH,

23   Germany).

24   Three ports were available at each of eight different depths (–0.01, –0.03, –0.05, –0.07, –0.10,

25   –0.20, –0.40, and –0.60 m): one inlet for the carrier gas, i.e., synthetic dry air (20.5 % O_2 in

26   N_2, with approx. 20-30 ppmv water vapor; Air Liquide, Germany), one sample air outlet, and

27   one duct for a soil temperature (T_S) sensor (type K thermocouple, Greisinger electronic

28   GmbH, Regenstauf, Germany; precision: 0.1°C). An additional fourth port at depths –0.01, –

29   0.03, –0.05, –0.10, –0.20, and –0.60 m was used for the measurement of soil volumetric water

30   content (θ) (EC-5, Decagon Devices, USA; precision: 0.02 m^3 m^{-3}).

1 At each depth inside the column a 0.15 m long piece of microporous polypropylene tubing

2 (Accurel® PP V8/2HF, Membrana GmbH, Germany; ~~0.155 cm~~1.55 10^{-3} m wall thickness,

3 ~~0.55 cm i.d., 0.86 cm o.d.)~~5.5 10^{-3} m inside diameter, 8.6 $10^{\wedge-3}$ m outside diameter) was

4 connected to the gas inlet and outlet port. The tubing offers the two advantages of being gas-

5 permeable (pore size of 0.2 ~~µm~~10^{-6} m) and exhibiting strong hydrophobic properties to

6 prevent liquid water from intruding into the tubing. It allows sampling of soil water vapor

7 and, hence, the determination of the isotope composition of soil liquid water (δ_{Sliq}) in a non-

8 destructive manner considering thermodynamic equilibrium between liquid and vapor phases

9 as detailed by Rothfuss et al. (2013).

10 ## 2.3 Internal isotope standards

11 Two internal standards ("st1" and "st2") were prepared using the same procedure as described

12 by Rothfuss et al. (2013). Two closed acrylic glass vessels (0.122 m i.d., 0.22 m height), in

13 each of which a 0.15 meter long piece of tubing as well as a type K thermocouple were

14 installed, were filled with FH31 sand (porosity = 0.34 m^3 m^{-3}, dry bulk density = 1.69 ~~g~~

15 ~~cm^3~~10^3 kg m^3, particle size distribution: 10% (> 0.5 ~~mm~~10^{-3} m), 72% (0.25- - 0.5 ~~mm~~10^{-3} m),

16 and 18% (< 0.25 ~~mm~~10^{-3} m)) (Merz et al., 2014; Stingaciu et al., 2009). Each vessel was

17 saturated with water of two different isotope compositions: δ^2H_{st1} = –53.51 (± 0.10) ‰,

18 $\delta^{18}O_{st1}$ = –8.18 (± 0.06) ‰ and δ^2H_{st2} = +15.56 (± 0.12) ‰, $\delta^{18}O_{st2}$ = +8.37 (± 0.04) ‰). Soil

19 water vapor from each vessel was sampled eight times per day for 30 min during the whole

20 experiment.

21 ## 2.4 Atmospheric measurements

22 Laboratory air was sampled passively with a 1/8" three meter-long stainless steel tubing at 2

23 m above the sand surface for isotope analysis of water vapor (δ_a). Air relative humidity (rh)

24 and temperature (T_a) were monitored at the same height with a combined rh and T_a sensor

25 (RFT-2, UMS GmbH, Germany; precision for rh and T_a were 2 % and 0.1°C, respectively).

26 Vapor pressure deficit (vpd) was calculated from rh and T_a data using the Magnus-Tetens

27 formula (Murray, 1967) for saturated vapor pressure. The laboratory was air-conditioned and

28 ventilated with seven axial fans (ETRI 148VK0281, 117 l s^{-1} airflow, ETRI/Rosenberg, USA)

29 positioned at 1.80 m height above the sand surface.

2.5 Sampling protocol and applied isotopic calibrations

The column was filled in a single step with FH31 sand and carefully shaken in order to reach a dry bulk density close to *in situ* field conditions. The sand was then slowly saturated from the bottom from an external water tank filled with st1 water on December 2, 2013. After saturation, the column was disconnected and sealed at the bottom using the two-way manual valve. It was finally installed on a balance (Miras 2 − 60EDL, Sartorius, USA), and let to evaporate for a period of 290 days in a ventilated laboratory.

δ_{Sliq} was determined in a sequential manner at each available depth once a day following the method developed by Rothfuss et al. (2013) (Fig. 1b). Dry synthetic air at a rate of 50 ml min^{-1} from a mass flow controller (EL-FLOW Analog, Bronkhorst High Tech, Ruurlo, The Netherlands) was directed to the permeable tubing for 30 minutes at each depth. The sampled soil water vapor was diluted with dry synthetic air provided by a second mass flow controller of the same type. This allowed (i) reaching a water vapor mixing ratio ranging between 17,000 and 23,000 ppmv (where L1102-i isotope measurements are most precise) and (ii) generating an excess flow downstream of the laser analyser. By doing this, any contamination of sample air with ambient air would be avoided. The excess flow was measured with a digital flow meter (ADM3000, Agilent Technologies, Santa Clara, CA, USA). The last 100 observations (corresponding to approx. 10 minutes) at steady state (standard deviations <0.70 ‰ and <0.20 ‰ for δ^2H and δ^{18}O, respectively) were used to calculate the raw isotope compositions of soil water vapor (δ_{Svap}). The latter was corrected for the water vapor mixing ratio dependence of the laser analyzer readings with 17,000 ppmv as reference level. Measurements that did not fulfil the above mentioned conditions for δ^2H and δ^{18}O standard deviations were not taken into account. Finally, these corrected values were used to infer the corresponding δ_{Sliq} at the measured T_S (Eq. (1) and (2); taken from Rothfuss et al., 2013):

$$\delta^2 H_{Sliq} = 104.96 - 1.0342 \cdot T_S + 1.0724 \cdot \delta^2 H_{Svap} \qquad (1)$$

$$\delta^{18} O_{Sliq} = 11.45 - 0.0795 \cdot T_S + 1.0012 \cdot \delta^{18} O_{Svap} \qquad (2)$$

The isotope composition of laboratory water vapor (δ_a) was measured eight times a day. δ_a, δ_{Svap}, and δ_{Sliq} values were finally corrected for laser instrument drift with time, using the isotope compositions of the two water standards, δ_{st1} and δ_{st2}.

Water vapor of the ambient air, of both standards, and from the different tubing sections in the soil column were sampled sequentially in the following order: soil (0.60 m) − soil (0.40 m) −

atmosphere – st1 – st2 – soil (0.20 m) – soil (0.10 m) – atmosphere – st1 – st2 – soil (0.07 m) – soil (0.05 m) – atmosphere – st1 – st2 – soil (0.03 m) – soil (0.01 m). Atmosphere water vapor was sampled twice as long (i.e., one hour) as soil water vapor from the column/standards so that each sequence lasted exactly 10 hours and started each day at the same time. The remaining 14 hours were used for additional standard and atmosphere water vapor measurements (i.e., on five occasions each).

2.6 Irrigation event

On Day of Experiment (DoE) 290 at 09:30 the sand surface was irrigated with 70 mm of st1 water. This was achieved over one hour in order to avoid oversaturation of the sand and avoid preferential pathways that would have affected the evaporation rate. For this, a 2 L polyethylene bottle was used. Its bottom was perforated with a set of 17 holes of 5 mm diameter and its cap with a single hole through which a PTFE bulkhead union tube fitting (Swagelok, USA) was installed. The bulkhead fitting was connected to a two-way needle valve (Swagelok, USA). Opening/closing the valve controlled the flow rate at which air entered the bottle headspace, which in turn controlled the irrigation flow rate.

To better observe the dynamics directly following the irrigation event, water vapor was sampled at a higher rate, i.e., 1, 3, 4, 5, 6, 9, 11, and 11 times per day at –0.60, –0.40, –0.20, –0.10, –0.07, –0.05, –0.03, and –0.01 m. Water vapor from both standards was sampled twice a day. The experiment was terminated after 299 days on September 26th, 2014.

2.7 Evaporation lines ~~(Craig and Gordon model, 1965)~~

Gat et al. (1971) proposed an expression based on the model of Craig and Gordon (1965) for the slope of the so-called "evaporation line" (S_{Ev}~~)~~, [-]) which quantifies the relative change in ~~δ^2H~~ δ^2H_{Sliq} and ~~$\delta^{18}O$~~ $\delta^{18}O_{Sliq}$ in a water body undergoing evaporation:

$$S_{Ev} = \frac{\Delta\!\left(\delta^2\mathrm{H}_{Sliq}\right)}{\Delta\!\left(\delta^{18}\mathrm{O}_{Sliq}\right)} = \frac{rh\cdot\left(\delta^2\mathrm{H}_a - \delta^2\mathrm{H}_{Sliq\_ini}\right) + \varepsilon_{eq}^{2H} + \Delta\varepsilon^{2H}}{rh\cdot\left(\delta^{18}\mathrm{O}_a - \delta^{18}\mathrm{O}_{Sliq\_ini}\right) + \varepsilon_{eq}^{18O} + \Delta\varepsilon^{18O}}$$

$$S_{Ev} = \frac{\Delta\!\left(\delta^2\mathrm{H}_{Sliq}\right)}{\Delta\!\left(\delta^{18}\mathrm{O}_{Sliq}\right)} = \frac{\left[rh\cdot\left(\delta_a - \delta_{Sliq\_ini}\right) + \varepsilon_{eq} + \Delta\varepsilon\right]_{2H}}{\left[rh\cdot\left(\delta_a - \delta_{Sliq\_ini}\right) + \varepsilon_{eq} + \Delta\varepsilon\right]_{18O}} \qquad (3)$$

~~where $\Delta\varepsilon^{2H}$ (resp. $\Delta\varepsilon^{18O}$) is the so-called "isotope kinetic effect" associated with $^1H^2H^{16}O$ (resp. $^1H_2^{18}O$) vapor transport:~~

11

1 ~~$\Delta\varepsilon^{2_H} = (1 - rh)\cdot\varepsilon_K^{2_H}$ (4a)~~

2 ~~$\Delta\varepsilon^{18_O} = (1 - rh)\cdot\varepsilon_K^{18_O}$ (4b)~~

3 ~~$\delta^2 H_{Sliq}$~~ with δ_{Sliq_ini} ~~(resp. $\delta^{18}O_{Sliq\_ini}$) is~~ the initial soil water (hydrogen or oxygen) liquid ~~$\delta^2 H$~~

4 ~~(resp. $\delta^{18}O$),~~ isotope composition, i.e., prior removal of water vapor by fractionating

5 evaporation. ~~$\varepsilon_{eq}^{2_H}$ (resp. $\varepsilon_{eq}^{18_O}$) and $\varepsilon_K^{2_H}$ (resp. $\varepsilon_K^{18_O}$) are the~~ ε_{eq} [-, expressed in ‰] is the

6 equilibrium ~~and kinetic~~ enrichment in either $^1H^2H^{16}O$ ~~(resp.~~ or $^1H_2^{18}O$~~) enrichments. $\varepsilon_{eq}^{2_H}$ (resp.~~

7 ~~$\varepsilon_{eq}^{18_O}$).~~ It is defined by the deviation from unity of the ratio between water and $^1H^2H^{16}O$ ~~(resp.~~

8 $^1H_2^{18}O)$~~ isotopologue saturated vapor pressures and can be calculated using the empirical

9 closed-form equations proposed by, e.g., Majoube (1971). ~~$\varepsilon_K^{2_H}$ (resp. $\varepsilon_K^{18_O}$)~~ $\Delta\varepsilon$ [-, expressed in

10 ‰] is ~~defined as~~ the ~~deviation from unity of the ratio between the resistance~~ so-called "isotope

11 kinetic effect" associated with ~~the transport of~~ $^1H^2H^{16}O$ ~~(resp.~~ and $^1H_2^{18}O)$ vapor ~~in the~~

12 ~~boundary air layer above the evaporating surface and that of water vapor. By~~

13 ~~assuming~~ transports. Assuming that (i) turbulent transport is a non-fractionating process and

14 ~~(considering that (ii) resistance associated with~~ the ratio of molecular diffusion ~~of $^1H^2H^{16}O$~~

15 ~~(resp. $^1H_2^{18}O$) vapor is inversely proportional~~ resistance to ~~the nth power of the corresponding~~

16 ~~diffusivity (D^{2_H}, resp. D^{18_O}),~~ total resistance equals one, it follows that (Gat, 2000):

17 $$\Delta\varepsilon = (1 - rh)\cdot\left(\frac{D^v}{D_i^v} - 1\right)\cdot n \qquad (4)$$

18 In Equation (4), the product $\left(\dfrac{D^v}{D_i^v} - 1\right)\cdot n$ is the isotope kinetic enrichment (ε_K, [-, expressed in

19 ‰]). In the present study, values for ratios of diffusivities (D^v/D_i^v) were taken from Merlivat

20 ~~and Coantic (1975) proposed the following expressions:~~ (1978):

21 ~~$\varepsilon_K^{2_H} = \left(\dfrac{D}{D^{2_H}}\right)^n - 1 = (1.0251)^n - 1$~~ $\begin{cases} \dfrac{D^v}{D_{2_H}^v} = 0.9755 \\ \dfrac{D^v}{D_{18_O}^v} = 0.9723 \end{cases}$ (5a~~)~~

22 ~~$\varepsilon_K^{18_O} = \left(\dfrac{D}{D^{18_O}}\right)^n - 1 = (1.0285)^n - 1$~~ (and 5b)

12

1 The ~~exponent~~term n accounts for the aerodynamic ~~regime above the liquid–vapor interface~~
2 ~~(i.e., where the relative humidity is 100%)~~ in the air boundary layer and ranges from $n_a = 0.5$
3 (~~fully~~ turbulent diffusion, i.e., atmosphere-controlled conditions) to $n_S = 1$ (~~fully~~
4 ~~diffusive~~molecular diffusion, i.e., soil-controlled conditions) with a value of ⅔ corresponding
5 to laminar flow conditions (Dongmann et al., 1974, Brutsaert, 1975). ~~In~~We tested the ~~present~~
6 ~~study, values for ratios of diffusivities (D/D^{2_H} and D/D^{18_O}) were taken from Merlivat (1978)~~
7 ~~and~~formulation proposed by Mathieu and Bariac (1996) where n ~~was~~is considered as a
8 function of soil water content ~~as proposed by Mathieu and Bariac (1996):~~:

9 $$n = \frac{(\theta_{surf} - \theta_{res}) \cdot n_a + (\theta_{sat} - \theta_{res}) \cdot n_S}{\theta_{sat} - \theta_{res}} \qquad (6)$$

10 with θ_{res}, θ_{sat}, and θ_{surf} the residual, saturated and surface soil water contents ~~(~~[$m^3\ m^{-3}$~~).~~].

11 Note that Equation (3) contrasts with the expression for the slope characterizing equilibrium
12 processes (e.g., precipitation formation) and therefore strictly temperature-dependant (i.e.,
13 $S_{eq} = \varepsilon_{eq}^{2_H} / \varepsilon_{eq}^{18_O}$). While S_{eq} might range for instance from 7.99 to 8.94 (for temperatures
14 spanning between 5 and 30°C), a much wider spread in S_{Ev} values is possible and has been
15 measured between 2 and 6 (Barnes and Allison, 1988, Brunel et al., 1995, DePaolo et al.,
16 2004).

17 ## 3 Results

18 ### 3.1 Example of a measuring sequence

19 Figure 2 shows exemplarily the measuring sequence for DoE 150. Soil and standards water
20 vapor mixing ratios were stable and ranged from 17,200 to 18,200 ppmv during the last 10
21 minutes of each sampling period (Fig. 2a). δ_{Svap} was within the range spanned by δ_{st1vap} and
22 δ_{st2vap} for both ^{2}H and ^{18}O (Fig. 2b). On DoE 150, the soil surface was sufficiently dry so that
23 atmospheric invasion of water vapor had started to significantly influence the δ_{Svap} of the
24 upper soil layers. Therefore, δ_{Svap} measured at –0.01 m was lower than at –0.03 m for both ^{2}H
25 and ^{18}O, but less pronounced for ^{2}H.

3.2   Time courses of air temperature, relative humidity and atmospheric δ^2H and δ^{18}O

During the experiment, the laboratory air temperature ranged from 15.6 to 22.5 °C (average: 18.7 ± 1.5 °C, Fig. 3a) and the relative humidity from 19 to 69 % (average: 40 % ± 0.08 %, Fig. 3a). Lower values of δ_a were observed from DoE 0 to 125 at lower air temperatures, whereas higher values occurred after DoE 125 at higher air temperatures (Fig. 3b).

3.3   Evolution of soil water content, temperature, evaporation flux, and δ_{Svap} from DoE 0-290

The soil temperature ranged from 16.2 to 22.3 °C (average: 18.6 ± 1.3 °C, data not shown) and closely followed that in the air, i.e., differences between daily mean soil and air temperatures ranged from -0.2 to 0.2 °C during the experiment. Following the saturation of the column, a strong decrease in water content was observed in the upper 10 cm, whereas after 287 days the sand was still saturated at –0.60 m (Fig. 4a). Figure 4b shows the time series of evaporation flux normalized by the vapor pressure deficit in the laboratory air (*Ev/vpd*, expressed in mm day^{-1} kPa^{-1}). *Ev/vpd* ratio was high at the beginning of the experiment, i.e., ranged from 2.44 to 3.22 mm d^{-1} kPa^{-1} during the first two experimental days. After DoE 180 and until the soil was irrigated, *Ev/vpd* stabilized to a mean value of 0.03 (±0.02) mm d^{-1} kPa^{-1}.

Due to fractionating evaporation flux, the δ_{Svap} of the topmost layer (–0.01 m) increased instantaneously (i.e., from DoE 0 onward) from the equilibrium δ_{Svap} value with the input water (–17.3 ‰ and –132.3 ‰ for ^{18}O and ^{2}H, respectively, at 16.5°C, Fig. 4c and d). Through back-diffusion of the excess heavy stable isotopologues from the evaporation front, δ_{Svap} measured at depths –0.03, –0.05, –0.07, –0.10, and –0.20 m departed from that same equilibrium value after 2, 3, 10, 25, and 92 days of the experiment, respectively. On the other hand, δ_{Svap} of the layers –0.40 and –0.60 m were constant over the entire duration of the experiment. Until DoE 65, the δ_{Svap} of the first 10 cm increased. From DoE 65 to 113 δ_{Svap} reached an overall stable value in the top layers –0.01 m (δ^2H$_{Svap}$ = 4.82 ± 2.06 ‰; δ^{18}O$_{Svap}$ = 11.72 ± 0.67 ‰) and –0.03 m (δ^2H$_{Svap}$ = 5.61 ± 3.14 ‰; δ^{18}O$_{Svap}$ = 10.41 ±0.81 ‰), whereas δ_{Svap} measured at depths –0.05, –0.07, and –0.10 m still progressively increased; from DoE 72 onward, δ_{Svap} at –0.20 m started to increase. δ^2H$_{Svap}$ and δ^{18}O$_{Svap}$ values started to decrease after about DoE 113 and DoE 155, respectively. δ^2H$_{Svap}$ at –0.01, –0.03, and –0.07 m on the

one hand and $\delta^{18}O_{Svap}$ at –0.01, –0.03, and –0.07 m on the other followed similar evolutions with maximum values measured below the surface down to –0.05 m.

3.4 Evolution of soil water content, temperature, evaporation flux, and δ_{Svap} from DoE 290 to 299

The layers –0.01, –0.03, –0.05, –0.10, and –0.20 m showed increases in θ of 0.31, 0.22, 0.30, 0.23, and 0.16 m^3 m^{-3} following irrigation, whereas θ at –0.60 m remained constant (Fig. 4e). $\theta_{-0.01m}$ and $\theta_{-0.03m}$ rapidly decreased down to values of 0.12 and 0.13 m^3 m^{-3}. Note that when $\theta_{-0.01m}$ and $\theta_{-0.03m}$ reached these values prior to irrigation, the evaporation rate was similar (i.e., $Ev/vpd = 0.65$ (± 0.12) mm d^{-1}, Fig. 4f).

Immediately after irrigation and for both isotopologues, δ_{Svap} at –0.01, –0.03, and –0.05 m was reset to a value close to that in equilibrium with st1 water (i.e., –17.8 ‰ and –132.0 ‰ for ^{18}O and ^{2}H, respectively, at 21.8 °C soil temperature, Fig. 4g and h). At –0.07 m, δ_{Svap} reached the above mentioned equilibrium values after about 3.5 days. δ_{Svap} at –0.20 m evolved in a similar way, whereas at –0.10 m the equilibrium values were reached after six hours. Finally, δ_{Svap} at –0.40 and –0.60 m and for both isotopologues were not affected by the water addition, which was consistent with the observed θ changes.

3.5 Evolution of soil temperature, water content, and δ_{Sliq} profiles

In Figure 5, T_S, θ, and δ_{Sliq} profiles for both isotopologues are plotted in three different panels, from DoE 0 to 100 (Fig. 5a-d, top panels), from DoE 101 to 287 (Fig. 5e-h, center panels), and from DoE 288 to 299 (Fig. 5i-l, bottom panels). The represented profiles were obtained from a linear interpolation of the times series of each variable. Thus, since the measuring sequence started each day at 08:00 and ended at 18:00, the depicted profiles are centered on 13:00.

Even if the soil temperature fluctuated during the course of the experiment, quasi-isothermal conditions were fulfilled at a given date, as the column was not isolated from its surroundings. On average, T_S only varied by 0.2 °C around the profile mean temperature at a given date. The δ_{Sliq} profiles showed a typical exponential shape from DoE 0 to approx. 100. Around DoE 100, when θ at –0.01 m reached a value of 0.090 m^3 m^{-3} (i.e., significantly greater than the sand residual water content $\theta = 0.035$ m^3 m^{-3}, determined by Merz et al. (2014)), the maximal δ_{Sliq} values were no longer observed at the surface and atmosphere water vapor started

1 invading the first centimeter of soil. Note that this happened slightly faster for $^1H^2H^{16}O$ than

2 for $^1H_2^{18}O$. On DoE 290, when the column was irrigated, the isotope profiles were partly reset

3 to their initial state, i.e., constant over depth and close to –53.5 and –8.2 ‰ for $^1H^2H^{16}O$ and

4 $^1H_2^{18}O$, respectively, with the exception of still enriched values at –0.07 m.

3.6 δ^2H-δ^{18}O relationships in soil water and atmosphere water vapor

6 Each plot of Figure 6 represents data of 50 consecutive days of the experiment. Laboratory

7 atmosphere water vapor δ^2H and δ^{18}O (gray symbols) were linearly correlated (linear

8 regression relationships in gray dotted lines) during the entire experiment (R^2 ranging

9 between 0.74 and 0.90, F-statistic p-value < 0.01), with the exception of the period DoE 125-

10 155 ($R^2 = 0.31$, p < 0.001), when atmospheric water ~~vapour~~vapor δ^2H was remarkably high in

11 the laboratory (Fig. 6c and d).

12 The linear regression slopes (LRS) between δ^2H_a and $\delta^{18}O_a$ ranged from 6.20 (DoE 50-100, p

13 < 0.01) to 8.29 (DoE 0-50, gray dotted line, p < 0.001). These values were significantly lower

14 than S_{eq}, the calculated ratio between the liquid-vapor equilibrium fractionations of $^1H^2H^{16}O$

15 and $^1H_2^{18}O$ (Majoube, 1971) that characterizes meteoric water bodies, which should have

16 ranged from 8.41 to 8.92 at the measured monthly mean atmosphere temperatures

17 (Forschungszentrum Jülich wheater station, 6°24'34" E, 50°54'36" N, 91 m.a.s.l.). Therefore,

18 it can be deduced that the laboratory air moisture was partly resulting from column

19 evaporation, typically leading to a δ^2H-δ^{18}O regression slope of lower than eight. This also

20 highlights the particular experimental conditions in the laboratory, where other sources of

21 water ~~vapour~~vapor (e.g., by opening the laboratory door) might have influenced the isotope

22 compositions of the air.

23 Considering all soil depths, the δ^2H_{Sliq}-$\delta^{18}O_{Sliq}$ LRS increased from 2.96 to 4.86 over the

24 course of the experiment (with $R^2 > 0.89$, p < 0.001). These values were much lower than that

25 of the slope of the Global Meteoric Water Line (GMWL, i.e., slope=8) also represented in

26 Figure 6. However, Figure 6 highlights the fact that in the upper three layers (–0.01, –0.03,

27 and –0.05 m) δ^2H_{Sliq}-$\delta^{18}O_{Sliq}$ LRS followed a significantly different evolution as the soil dried

28 out. Figure 7 shows average δ^2H-δ^{18}O LRS calculated for time intervals of ten consecutive

29 days for the atmosphere (gray line), the three upper layers (colored solid lines), and the

30 remaining deeper layers (–0.07, –0.10, –0.20, –0.40, and –0.60 m, black dotted line). While

31 both δ^2H-δ^{18}O LRS in the atmosphere and in the first three depths fluctuated during the

1   experiment, the LRS of the combined remaining deeper layers varied only little between 3.07

2   and 4.49 (average = 3.78 ± 0.54). From DoE 150, δ^2H-δ^{18}O LRS of the atmosphere and at −

3   0.01, –0.03, and –0.05 m were linearly correlated (R^2 = 0.73, 0.48, and 0.42, with p < 0.001, <

4   0.01, and < 0.05, respectively), whereas they were not correlated before DoE 125,

5   demonstrating again the increasing influence of the atmosphere (atmosphere invasion) on the

6   soil surface layer as the EF receded in the soil. Note the negative δ^2H$_a$-δ^{18}O$_a$ LRS (R^2 = 0.26,

7   p < 0.001) observed between DoE 125 and 150, due to remarkably high atmosphere vapor

8   δ^2H measured in the laboratory.

9

4   Discussion

4.1   Long term reliability of the method

12 The method proved to be reliable in the long term as the tubing sections positioned at –0.60

13 and –0.40 m (i.e., where the sand was saturated or close to saturation during the entire

14 experiment) remained watertight even after 299 days. As demonstrated by Rothfuss et al.

15 (2013), (i) the length of the gas-permeable tubing, (ii) the low synthetic dry air flow rate, and

16 (iii) the daily measurement frequency allowed removing soil water vapor which remained

17 under thermodynamic equilibrium with the soil moisture. Moreover, this was also true for the

18 upper soil layers even at low soil water content: steady values for water vapor mixing ratio

19 and isotope compositions were always reached during sampling throughout the experiment.

20 Finally, our method enabled inferring the isotope composition of tightly bound water at the

21 surface. This would be observable by the traditional vacuum distillation method with certainly

22 a lower vertical resolution due to low moisture content. As also pointed out by Rothfuss et al.

23 (2013), it can be assumed that the sand properties did not cause any fractionation of pore

24 water ^{2}H and ^{18}O. In contrast, this could not be the case in certain soils with high cation

25 exchange capacity (CEC) as originally described by Sofer and Gat (1972) and recently

26 investigated by Oerter et al. (2014).

4.2   Locating the evaporation front depth from soil water δ^2H and δ^{18}O profiles

28 From Figure 4b no distinct characteristic evaporation stages, i.e., stages I and II referring to

29 atmosphere-controlled and soil-controlled evaporation phases, respectively, could be

30 identified. The opposite was observed by Merz et al. (2014), who conducted an evaporation

1   study using the same sand. This indicates greater wind velocity in the air layer above the soil

2   column due to the laboratory ventilation. For higher wind velocities, the boundary layer above

3   the drying medium is thinner and the transfer resistance for vapor transfer lower than for

4   lower wind velocities. But, for thinner boundary layers, the evaporation rates depends

5   stronger on the spatial configuration of the vapor field above the partially wet evaporating

6   surface. This makes that the evaporation rate decreases and the transfer resistance in the

7   boundary layer increases more in relative terms with decreasing water content of the

8   evaporation surface for higher than for lower wind velocities (Shahraeeni et al., 2012).

9   Locating the EF in the soil is of importance for evapotranspiration partitioning purposes: from

10   the soil water isotope composition at the EF, it is possible to calculate the evaporation flux

11   isotope composition using the Craig and Gordon formula (Craig and Gordon, 1965). For a

12   uniform isotope diffusion coefficient distribution in the liquid phase, an exponential decrease

13   of the isotope composition gradient with depth is expected. However, when evaporation and

14   thus accumulation of isotopologues occur in a soil layer between two given observation

15   points, then the isotope gradient between these two points is smaller than the gradient deeper

16   in the profile. Therefore we can consider the time when the isotope composition gradient is no

17   longer the largest between these two upper observation depths as the time when the EF moves

18   into the soil layer below.

19   Figure 8a and b display the evolutions of the isotope compositions gradients $d(\delta^{18}O_S)/dz$ and

20    $d(\delta^2 H_S)/dz$ calculated between two consecutive observation points in the soil (i.e., between

21   –0.01 and –0.03 m in brown solid line, between –0.03 and –0.05 m in red solid line, etc.).

22   Figure 8c translates these isotope gradients in terms of EF depths ($z^{18}O_{EF}$ and z^2H_{EF},

23   respectively). Each day, the maximum $d(\delta^{18}O_S)/dz$ and $d(\delta^2 H_S)/dz$ define the layer where

24   evaporation occurs, e.g., when $d(\delta^{18}O_S)/dz$ is maximal between –0.01 and –0.03 m on a given

25   DoE, $z^{18}O_{EF}$ is estimated to be greater than –0.01 m and is assigned the value of 0 m.

26   When $d(\delta^{18}O_S)/dz$ is maximal between –0.03 and –0.05 m on a given DoE, $z^{18}O_{EF}$ is

27   estimated to range between –0.01 and –0.03 m and is assigned the value –0.02 m. From

28   both $d(\delta^{18}O_S)/dz$ and $d(\delta^2 H_S)/dz$, a similar evolution of the depth of the evaporation front

29   was derived despite the fact that $\delta^2 H_{Sliq}$ and $\delta^{18}O_{Sliq}$ time courses were different and showed

30   maxima at different times. It was inferred that after 290 days under the prevailing laboratory

1   air temperature, moisture, and aerodynamic conditions, and given the specific hydraulic

2   properties of the sand, the EF had moved down to an approximate depth of –0.06 m.

3   ~~**4.3 Testing the Craig and Gordon (1965) relationship with isotope data**~~

4   **4.3   Isotope kinetic effects during soil evaporation**

5   For each period of ten consecutive days the minimum measured $\delta^2 H_{Sliq}$ and $\delta^{18}O_{Sliq}$ provided

6   $\delta^2 H_{Sliq\_ini}$ and $\delta^{18}O_{Sliq\_ini}$ in Equation (3). $\delta^2 H_a$ and $\delta^{18}O_a$ were obtained from the mean values

7   of their respective times series. Mean soil surface water content (θ_{surf}) measured in the layer

8   above the EF (as identified in section 4.2) provided the n parameter in Equation (6) and

9   ultimately ε_K^{2H} and ε_K^{18o} (Eq. (5a) and (5b)). ε_{eq}^{2H} and ε_{eq}^{18o} were calculated from Majoube (1971)

10   at the mean soil temperature measured at z_{EF}. Relative humidity was normalized to the soil

11   temperature measured at the EF. Finally, standard error for S_{Ev} was obtained using an

12   extension of the formula proposed by Phillips and Gregg (2001) and detailed by Rothfuss et

13   al. (2010). For this, standard errors associated with the determination of the variables in

14   Equation (3) were taken equal to their measured standard deviations for each time period.

15   Standard errors for the parameters θ_{res} and θ_{sat} were set ~~arbitrarily~~ to 0.01 m^3 m^{-3} (i.e.,

16   comparable to the soil water content probes' precision) and for the diffusivity ratios

17   D/D^{2H} and D/D^{18o} to zero (i.e., no uncertainty about their value was taken into account,

18   although debatable, e.g., Cappa et al., 2003).

19   Figure 9a shows the comparison between time courses of S_{Ev} and $\delta^2 H_{Sliq}$-$\delta^{18}O_{Sliq}$ LRS

20   computed with data below the EF. Both ranged between 2.9 and 4.8, i.e., within the range of

21   reported values (e.g., Barnes and Allison, 1988, Brunel et al., 1995, DePaolo et al., 2004).

22   Note that both observed and simulated slopes' values increased over time, even though the

23   ~~boundary~~ air layer above the EF gradually thickened as the soil dried out. The opposite was

24   observed by e.g., Barnes and Allison (1983), who simulated isotopic profiles at steady state

25   with constant relative humidity. In the present study however the atmosphere relative

26   humidity gradually increased which in turn decreased the kinetic effects associated with

27   $^1H^2H^{16}O$ and $^1H_2^{18}O$ ~~vapour~~vapor transports and thus increased slopes over time. The general

28   observed trend was very well reproduced by the model between DoE 30 and 150 (Nash and

29   Sutcliffe Efficiency - NSE = 0.92; Nash and Sutcliffe, 1970), whereas S_{Ev} departed from data

30   from DoE 150 onwards (NSE < 0). Overall, the Craig and Gordon (1965) model could

1   explain about 62 % of the data variability with a Root Mean Square Error (RMSE) of 0.58

2   (and 76 % when data from the period DoE 0-10 is left out, p-value < 0.001, RMSE = 0.52). At

3   the beginning of the experiment (DoE 0-20), simulated values were greater than computed

4   δ^2H-$\delta^{18}O$ LRS, even when taking into account the high S_{Ev} standard errors due to fast

5   changing θ_{surf} (Phillips and Gregg, 2001). Although S_{Ev} was equal to 3.8 for the period DoE 0-

6   10, δ^2H-$\delta^{18}O$ LRS had already reached down a value of 2.9, meaning that the EF should have

7   been no longer at the surface (i.e., between the surface and 0.01 m depth) leading to greater n,

8   therefore lower slope value.

9   After DoE 150 and until DoE 290 when evaporation flux was lower than 0.40 mm d^{-1},

10   difference between model and data progressively increased. For a better model-to-data fit, the

11    $^1H^2H^{16}O$ and $^1H_2^{18}O$ kinetic effects should decrease, through either (i) decrease of ~~ε_K (i.e.,~~

12   ~~decrease of n),~~n, which is from a theoretical point of view counter-intuitive and e.g.,

13   contradicts the formulation of Mathieu and Bariac (1996) or (ii) decrease of term $(1 - rh)$, or

14   else (iii) a combination of (i) and (ii). In another laboratory study where $\delta^{18}O$ of water in bare

15   soil columns was measured destructively and $\delta^{18}O$ of evaporation was estimated from

16   cryoscopic trapping of water ~~vapour~~vapor at the outlet of the columns' headspaces, Braud et

17   al. (2009a and b) could capture $\varepsilon_K^{18_O}$ dynamics by inverse modelling. In their case, $\varepsilon_K^{18_O}$

18   generally reached values close to $\varepsilon_K^{18_O} = 18.9‰$ corresponding to laminar conditions above the

19   liquid-vapor interface (n = 2/3). They however determined at the end of their experiments,

20   when the soil surface dry layer thickened and soil surface relative humidity was significantly

21   lower than 100%, values lower than reported in the literature (i.e., $\varepsilon_K^{18_O} < 14.1‰$). These

22   results were partly explained by the particular experimental conditions leading to

23   uncertainties in characterizing evaporation isotope compositions when the dry soil surface

24   layer was the most developed. Nevertheless, the same observation could be made in the

25   present study while having a different soil texture (silt loam *versus* quartz sand) and

26   noticeable different atmospheric conditions ("free" laboratory atmosphere *versus* sealed

27   headspace circulated with dry air). Figure 9c displays the evolution of $\varepsilon_K^{2_H}$ (resp. $\varepsilon_K^{18_O}$) that

28   provided the best fit with data (NSE = 0.99) through fitting of the n parameter (shown Figure

29   9b) instead of calculating it with Equation (6). In this scenario, n decreased from one to 0.59,

30   with a mean value of 0.96 ± 0.03 during the period DoE 0-150.

1   Instead of changing the value of n over time (and therefore those of ε_K^{2H} and ε_K^{18O}), another

2   possibility is to consider that after some time the relative humidity at the EF (rh_{EF}) was

3   different from 100%, although the EF was still at thermodynamic equilibrium. In that case

4   kinetic effects would have depended on the difference ($rh_{EF} - rh$) instead of ($1 - rh$). Figure

5   9b shows the rh_{EF} time course that provided the best model-to-data fit (NSE = 0.92), when

6   ε_K^{2H} and ε_K^{18O} were calculated (Eq. (5a-5b-6)). In this second scenario, rh_{EF} decreased from 100

7   to 81 % with a mean value of 99.5 ± 0.03 % for the period DoE 0-150, i.e., in a similar

8   fashion than fitted n values obtained in the 1st scenario. These values were significantly lower

9   than what is calculated with Kelvin's Equation linking rh_{EF} with soil water tension at the EF

10   in the case of liquid-vapor equilibrium, which for the soil retention properties (Merz et al.,

11   2014) would range between 100 and 99.6 %. In a third scenario one could consider a

12   combined decrease of n and rh_{EF} to smaller extents, for which there are no unique solutions at

13   each time step. In a fourth scenario, the ratio of turbulent diffusion resistance to molecular

14   diffusion resistance is no more negligible, leading to n' values ranging between 0 and n

15   (Merlivat and Jouzel, 1979). This last scenario was however not verifiable. In any case, only

16   decreasing kinetic effects could provide a better model-to-data fit. Note that the formulation

17   of kinetic enrichments proposed by Merlivat and Coantic (1975) and based on the evaporation

18   model of Brutsaert (1982) was not tested due to lack of appropriate data (i.e., unknown wind

19   distribution profile over the soil column). The formulations of Melayah et al. (1996) (n = 0)

20   and Barnes and Allison (1983) (n = 1) were also not tested as they give kinetic enrichments

21   constant over time and cannot explain a change of S_{Ev} value through change of n. Finally, S_{Ev}

22   calculations using diffusivity ratios determined by Cappa et al. (2003) lead to lower value of

23   S_{Ev} and less good model-to-data fit.

24   In the present study, information on δ^2H and $\delta^{18}O$ of the evaporation flux was missing to

25   address uncertainties in the determination of ε_K^{2H} and ε_K^{18O}. The experimental setup would also

26   have gained from the addition of appropriate sensors (e.g., micro-psychrometers) to measure

27   the soil surface relative humidity and especially rh_{EF}, although the dimensions of the column

28   would certainly be a limiting factor. Finally note that S_{Ev} calculations using diffusivity ratios

29   determined by Cappa et al. (2003) lead to lower value of S_{Ev} and less good model-to-data fit.

30   A more in depth investigation of the behavior of S_{Ev} (and isotope composition gradients with

31   depth for that matter) with time could be carried out with detailed numerical simulations using

32   an isotope-enabled SVAT model such as SiSPAT-Isotope.

5 Conclusion

Since the initial work of Zimmermann et al. (1967), water stable isotopologues have proven both theoretically and experimentally to be valuable tools for the study of water flow in the soil and at the soil-atmosphere interface. In this work we present the first application of the method of Rothfuss et al. (2013). This study constitutes also the very first long-term application of the series of newly developed isotopic monitoring systems based on gas-permeable tubing and isotope-specific infrared laser absorption spectroscopy (Herbstritt et al., 2012; Volkmann and Weiler, 2014).Our method proved to be reliable over long time periods and followed quantitatively the progressive isotope enrichment caused by evaporation in an initially saturated soil column. Moreover, it could capture sudden variations following a simulated intense rain event.

Simple calculations of isotope compositions' gradients made it possible to evaluate the position of the Evaporation Front and observe how it progressively receded with time in the soil. Confrontation of the model of Craig and Gordon (1965) with data also highlighted uncertainties associated with the determinations of isotope kinetic fractionations and soil relative humidity at the EF when the soil surface dry layer was the most developed and evaporation flux was low.

Our method will allow experimentalists to measure and locate the evaporation front in a dynamic and non-destructive manner and to calculate the isotope compositions of the evaporation flux using the model of Craig and Gordon (1965) with much higher time resolution. Provided that the isotope compositions of evapotranspiration and transpiration fluxes are measured or modelled, this method will be especially useful to test hypotheses and improve our understanding of root water uptake processes and the partitioning of evapotranspiration fluxes.

1 **References**

2 Barnes, C. J., and Allison, G. B.: The Distribution of Deuterium and O-18 in Dry Soils .1.

3 Theory, J. Hydrol., 60, 141-156, doi: 10.1016/0022-1694(83)90018-5, 1983.

4 Barnes, C. J., and Allison, G. B.: The Distribution of Deuterium and O-18 in Dry Soils .3.

5 Theory for Non-Isothermal Water-Movement, J. Hydrol., 74, 119-135, doi: 10.1016/0022-

6 1694(84)90144-6, 1984.

7 Barnes, C. J., and Allison, G. B.: Tracing of water movement in the unsaturated zone using

8 stable isotopes of hydrogen and oxygen, J. Hydrol., 100, 143–176, doi:10.1016/0022-

9 1694(88)90184-9, 1988

10 Barnes, C. J., and Walker, G. R.: The Distribution of Deuterium and O-18 during Unsteady

11 Evaporation from a Dry Soil, J. Hydrol., 112, 55-67, doi: 10.1016/0022-1694(89)90180-7,

12 1989.

13 Blasch, K. W., and Bryson, J. R.: Distinguishing sources of ground water recharge by using

14 delta H-2 and delta O-18, Ground Water, 45, 294-308, doi: 10.1111/j.1745-

15 6584.2006.00289.x, 2007.

16 Braud, I., Bariac, T., Gaudet, J. P., and Vauclin, M.: SiSPAT-Isotope, a coupled heat, water

17 and stable isotope (HDO and (H2O)-O-18) transport model for bare soil. Part I. Model

18 description and first verifications, J. Hydrol., 309, 277-300, doi:

19 10.1016/j.jhydrol.2004.12.013, 2005.

20 Braud, I., Biron, P., Bariac, T., Richard, P., Canale, L., Gaudet, J. P., and Vauclin, M.:

21 Isotopic composition of bare soil evaporated water vapor. Part I: RUBIC IV experimental

22 setup and results, J. Hydrol., 369, 1-16, DOI 10.1016/j.jhydrol.2009.01.034, 2009a.

23 Braud, I., Bariac, T., Biron, P., and Vauclin, M.: Isotopic composition of bare soil evaporated

24 water vapor. Part II: Modeling of RUBIC IV experimental results, J. Hydrol., 369, 17-29,

25 DOI 10.1016/j.jhydrol.2009.01.038, 2009b.

26 Brunel, J. P., Walker, G. R, and Kennettsmith, A. K.: Field Validation of Isotopic Procedures

27 for Determining Sources of Water Used by Plants in a Semiarid Environment, J. Hydrol., 167,

28 351-368, doi: 10.1016/0022-1694(94)02575-V, 1995.

24

1 Brutsaert, W.: A theory for local evaporation (or heat transfer) from rough and smooth
2 surfaces at ground level, Water Resour. Res., 11, 543-550, doi: 10.1029/WR011i004p00543,
3 1975.

4 Craig, H.: Isotopic Variations in Meteoric Waters, Science, 133, 1702-1703, doi:
5 10.1126/science.133.3465.1702, 1961.

6 Craig, H., and Gordon, L. I.: Deuterium and oxygen 18 variations in the ocean and marine
7 atmosphere, Stable Isotopes in Oceanographic Studies and Paleotemperatures, Spoleto, Italy,
8 1965, 9-130, 1965.

9 DePaolo, D. J., Conrad, M. E., Maher, K., and Gee, G. W.: Evaporation effects on oxygen and
10 hydrogen isotopes in deep vadose zone pore fluids at Hanford, Washington, Vad. Zone. J., 3,
11 220-232, doi:10.2113/3.1.220, 2004.

12 Dongmann, G., H. W. Nurnberg, H. Forstel, and Wagener, K.: Enrichment of $H_2^{18}O$ in
13 Leaves of Transpiring Plants, Radiat Environ Bioph, 1, 41-52, doi: 10.1007/Bf01323099,
14 1974.

15 Dubbert, M., Cuntz, M., Piayda, A., Maguás, C., and Werner, C.: Partitioning
16 evapotranspiration – Testing the Craig and Gordon model with field measurements of oxygen
17 isotope ratios of evaporative fluxes, J. Hydrol., 496, 142-153, doi:
18 10.1016/j.jhydrol.2013.05.033, 2013.

19 Gaj, M., Beyer, M., Koeniger, P., Wanke, H., Hamutoko, J., and Himmelsbach, T.: In-situ
20 unsaturated zone stable water isotope (2H and 18O) measurements in semi-arid environments
21 using tunable off-axis integrated cavity output spectroscopy, Hydrol. Earth Syst. Sci. Discuss.
22 12, 6115-6149, doi:10.5194/hessd-12-6115-2015, 2015.

23 Gat, J.: Comments on the Stable Isotope Method in Regional Groundwater Investigations,
24 Water Resour. Res., 7, 980-993, doi: 10.1029/WR007i004p00980, 1971

25 Gat, J. R.: Atmospheric water balance - the isotopic perspective, Hydrol. Process., 14, 1357-
26 1369, doi: 10.1002/1099-1085, 2000.

27 Goldsmith, G.R., Munoz-Villers, L.E., Holwerda, F., McDonnell, J.J., Asbjornsen, H.,
28 Dawson, T.E.: Stable isotopes reveal linkages among ecohydrological processes in a
29 seasonally dry tropical montane cloud forest, Ecohydrology, 5, 779-790, doi:
30 10.1002/eco.268, 2011.

1 Gonfiantini, R.: Standards for stable isotope measurements in natural compounds, Nature,
2 271, 534-536, doi: 10.1038/271534a0, 1978.

3 Haverd, V., and Cuntz, M.: Soil-Litter-Iso: A one-dimensional model for coupled transport of
4 heat, water and stable isotopes in soil with a litter layer and root extraction, J. Hydrol., 388,
5 438-455, doi: 10.1016/j.jhydrol.2010.05.029, 2010.

6 Herbstritt, B., Gralher, B., and Weiler, M.: Continuous in situ measurements of stable
7 isotopes in liquid water, Water Resour. Res., 48, doi: 10.1029/2011wr011369, 2012.

8 Hu, Z. M., Wen, X. F., Sun, X. M., Li, L. H., Yu, G. R., Lee, X. H., and Li, S. G.: Partitioning
9 of evapotranspiration through oxygen isotopic measurements of water pools and fluxes in a
10 temperate grassland, J Geophys Res-Biogeo, 119, 358-371, doi: 10.1002/2013jg002367,
11 2014.

12 Jasechko, S., Sharp, Z. D., Gibson, J. J., Birks, S. J., Yi, Y., and Fawcett, P. J.: Terrestrial
13 water fluxes dominated by transpiration, Nature, 496, 347-351, doi: 10.1038/Nature11983,
14 2013.

15 Litaor, M.I.: Review of Soil Solution Samplers. Water Resour. Res., 24, 727-733, doi:
16 10.1029/Wr024i005p00727, 1988

17 Liu, Z. F., Bowen, G. J., and Welker, J. M.: Atmospheric circulation is reflected in
18 precipitation isotope gradients over the conterminous United States, J. Geophys. Res.-Atmos.,
19 115, doi: 10.1029/2010jd014175, 2010.

20 Melayah, A., Bruckler, L., and Bariac, T.: Modeling the transport of water stable isotopes in
21 unsaturated sails under natural conditions .1. Theory, Water Resour. Res., 32, 2047-2054, doi:
22 10.1029/96wr00674, 1996.

23 Merlivat, L.: Molecular Diffusivities of H216O, HD16O, and H218O in Gases, J. Chem.
24 Phys., doi: 10.1063/1.436884, 1978

25 Merlivat, L., and Coantic, M.: Study of Mass-Transfer at Air-Water-Interface by an Isotopic
26 Method, J. Geophys. Res.-Oc. Atm., 80, 3455-3464, doi: 10.1029/Jc080i024p03455, 1975

27 Merlivat, L., and Jouzel, J.: Global Climatic Interpretation of the Deuterium-Oxygen-18
28 Relationship for Precipitation, J Geophys Res-Oc Atm, 84, 5029-5033, doi:
29 10.1029/JC084iC08p05029, 1979.

1 Majoube, M.: Oxygen-18 and Deuterium Fractionation between Water and Steam, J. Chim.
2 Phys. Phys.-Chim. Biol., 68, 1423-1436, 1971.

3 Mathieu, R., and Bariac, T.: A numerical model for the simulation of stable isotope profiles in
4 drying soils, 101, 12685–12696, J. Geophys. Res.-Atmos., doi: 10.1029/96jd00223, 1996

5 Merz, S., Pohlmeier, A., Vanderborght, J., van Dusschoten, D., and Vereecken, H.: Moisture
6 profiles of the upper soil layer during evaporation monitored by NMR, Water Resour. Res.,
7 50, 5184-5195, doi: 10.1002/2013wr014809, 2014.

8 Murray, F. W.: On the Computation of Saturation Vapor Pressure, J. Appl. Meteorol., 6, 203-
9 204, doi: 10.1175/1520-0450, 1967.

10 Nash, J. E., and Sutcliffe, J. V.: River flow forecasting through conceptual models part I -A
11 discussion of principles, Journal of Hydrology, 10, 282-290, doi:10.1016/0022-
12 1694(70)90255-6, 1970

13 Oerter, E., Finstad, K., Schaefer, J., Goldsmith, G. R., Dawson, T., and Amundson, R.:
14 Oxygen isotope fractionation effects in soil water via interaction with cations (Mg, Ca, K, Na)
15 adsorbed to phyllosilicate clay minerals, J. Hydrol., 515, 1-9, doi:
16 10.1016/j.jhydrol.2014.04.029, 2014.

17 Peng, T. R., Lu, W. C., Chen, K. Y., Zhan, W. J., and Liu, T. K.: Groundwater-recharge
18 connectivity between a hills-and-plains' area of western Taiwan using water isotopes and
19 electrical conductivity, J. Hydrol., 517, 226-235, doi: 10.1016/j.jhydrol.2014.05.010, 2014.

20 Phillips, D. L., and Gregg, J. W.: Uncertainty in source partitioning using stable isotopes,
21 Oecologia, 127, 171-179, doi: 10.1007/s004420000578, 2001.

22 Rothfuss, Y., Biron, P., Braud, I., Canale, L., Durand, J. L., Gaudet, J. P., Richard, P.,
23 Vauclin, M., and Bariac, T.: Partitioning evapotranspiration fluxes into soil evaporation and
24 plant transpiration using water stable isotopes under controlled conditions, Hydrol. Process.,
25 24, 3177-3194, doi: 10.1002/Hyp.7743, 2010.

26 Rothfuss, Y., Braud, I., Le Moine, N., Biron, P., Durand, J. L., Vauclin, M., and Bariac, T.:
27 Factors controlling the isotopic partitioning between soil evaporation and plant transpiration:
28 Assessment using a multi-objective calibration of SiSPAT-Isotope under controlled
29 conditions, J. Hydrol., 442, 75-88, doi: 10.1016/j.jhydrol.2012.03.041, 2012.

1 Rothfuss, Y., Vereecken, H., and Brüggemann, N.: Monitoring water stable isotopic
2 composition in soils using gas-permeable tubing and infrared laser absorption spectroscopy,
3 Water Resour. Res., 49, 1-9, doi: 10.1002/wrcr.20311, 2013.

4 Schmidt, M., Maseyk, K., Lett, C., Biron, P., Richard, P., Bariac, T., and Seibt, U.:
5 Concentration effects on laser-based d18O and d2H measurements and implications for the
6 calibration of vapour measurements with liquid standards, Rapid Commun. Mass Spectrom,
7 24, 3553–3561, doi: 10.1002/rcm.4813, 2010.

8 Shahraeeni, E., Lehmann, P., and Or, D.: Coupling of evaporative fluxes from drying porous
9 surfaces with air boundary layer: Characteristics of evaporation from discrete pores, Water
10 Resour. Res., 48, doi: 10.1029/2012wr011857, 2012.

11 Singleton, M. J., Sonnenthal, E. L., Conrad, M. E., DePaolo, D. J., and Gee, G. W.:
12 Multiphase reactive transport modeling of seasonal infiltration events and stable isotope
13 fractionation in unsaturated zone pore water and vapor at the Hanford site, Vadose Zone J., 3,
14 775-785, doi: 10.2113/3.3.775, 2004.

15 Sofer, Z., and Gat, J. R.: Activities and Concentrations of O-18 in Concentrated Aqueous Salt
16 Solutions - Analytical and Geophysical Implications, Earth Planet. Sc. Lett., 15, 232-&, doi:
17 10.1016/0012-821x(72)90168-9, 1972.

18 Stingaciu, L. R., Pohlmeier, A., Blumler, P., Weihermuller, L., van Dusschoten, D., Stapf, S.,
19 and Vereecken, H.: Characterization of unsaturated porous media by high-field and low-field
20 NMR relaxometry, Water Resour. Res., 45, doi: 10.1029/2008wr007459, 2009.

21 Sutanto, S. J., Wenninger, J., Coenders-Gerrits, A. M. J., and Uhlenbrook, S.: Partitioning of
22 evaporation into transpiration, soil evaporation and interception: a comparison between
23 isotope measurements and a HYDRUS-1D model, Hydrol. Earth Syst. Sc., 16, 2605-2616,
24 doi: 10.5194/hess-16-2605-2012, 2012.

25 Volkmann, T. H. M., and Weiler, M.: Continual in situ monitoring of pore water stable
26 isotopes in the subsurface, Hydrol. Earth Syst. Sc., 18, 1819-1833, doi: 10.5194/hess-18-
27 1819-2014, 2014.

28 Wang, P., Song, X. F., Han, D. M., Zhang, Y. H., and Liu, X.: A study of root water uptake of
29 crops indicated by hydrogen and oxygen stable isotopes: A case in Shanxi Province, China,
30 Agric. Water Manage., 97, 475-482, doi: 10.1016/j.agwat.2009.11.008, 2010.

1 Yepez, E. A., Huxman, T. E., Ignace, D. D., English, N. B., Weltzin, J. F., Castellanos, A. E.,

2 and Williams, D. G.: Dynamics of transpiration and evaporation following a moisture pulse in

3 semiarid grassland: A chamber-based isotope method for partitioning flux components, Agr.

4 Forest Meteorol., 132, 359-376, doi: 10.1016/j.agrformet.2005.09.006, 2005.

5 Zimmermann, U., Ehhalt, D., and Münnich, K. O.: Soil water movement and

6 evapotranspiration: changes in the isotopic composition of the water, Symposium of Isotopes

7 in Hydrology, Vienna, 1967, 567–584.

1 Figures
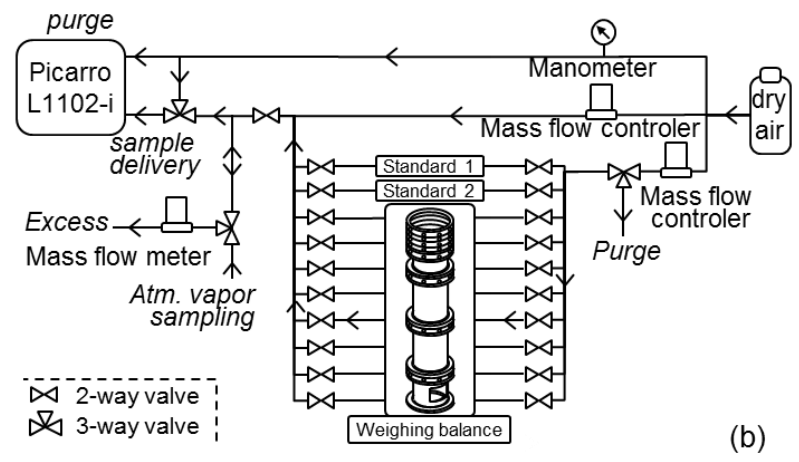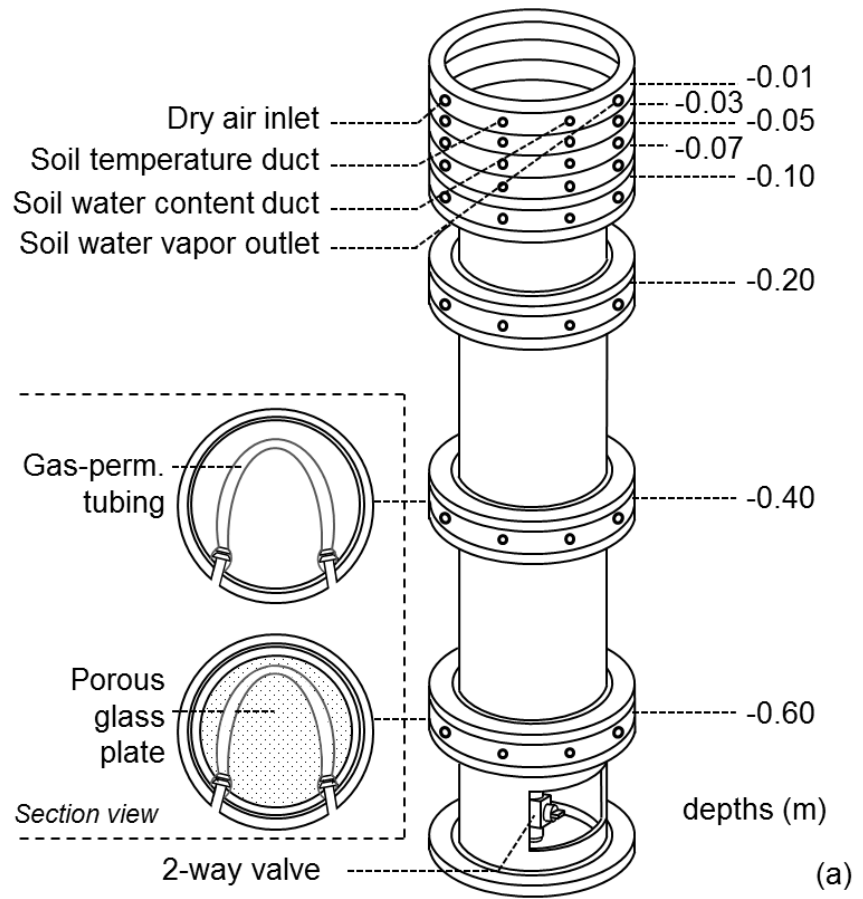
2

3   Figure 1. (a) Scheme of the acrylic glass column used in the experiment; (b) experimental setup for sampling water vapor at the different soil

4   depths of the soil column, from the ambient air, and from the two soil water standards (standard 1 and 2)
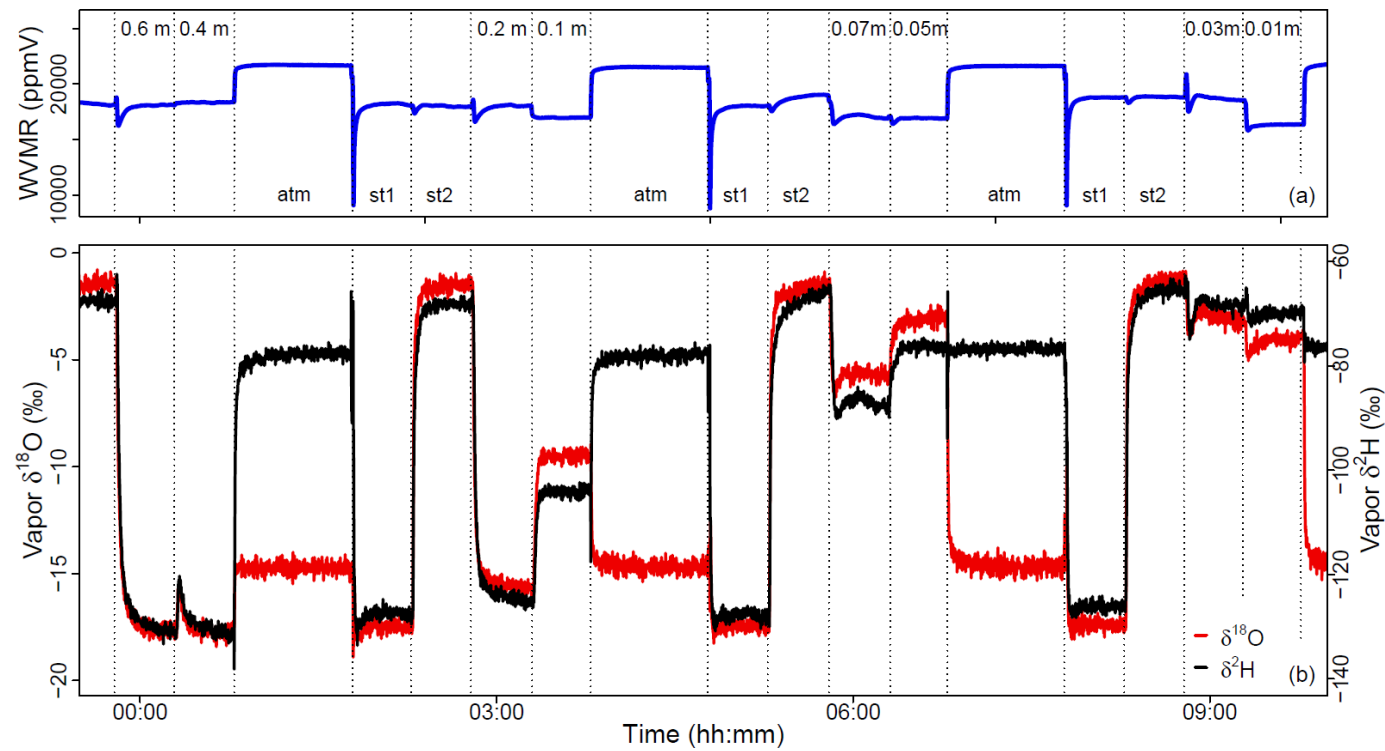
5

Figure 2. Water vapor mixing ratio (*WVMR*, in ppmv) and isotope composition ($\delta^{18}O$ and $\delta^{2}H$, in ‰ V-SMOW) of the water vapor sampled on Day of Experiment 150 from the ambient air ("atm"), both standards ("st1" and "st2"), and from the tubing sections at soil depths 1, 3, 5, 7, 10, 20, 40, and 60 cm
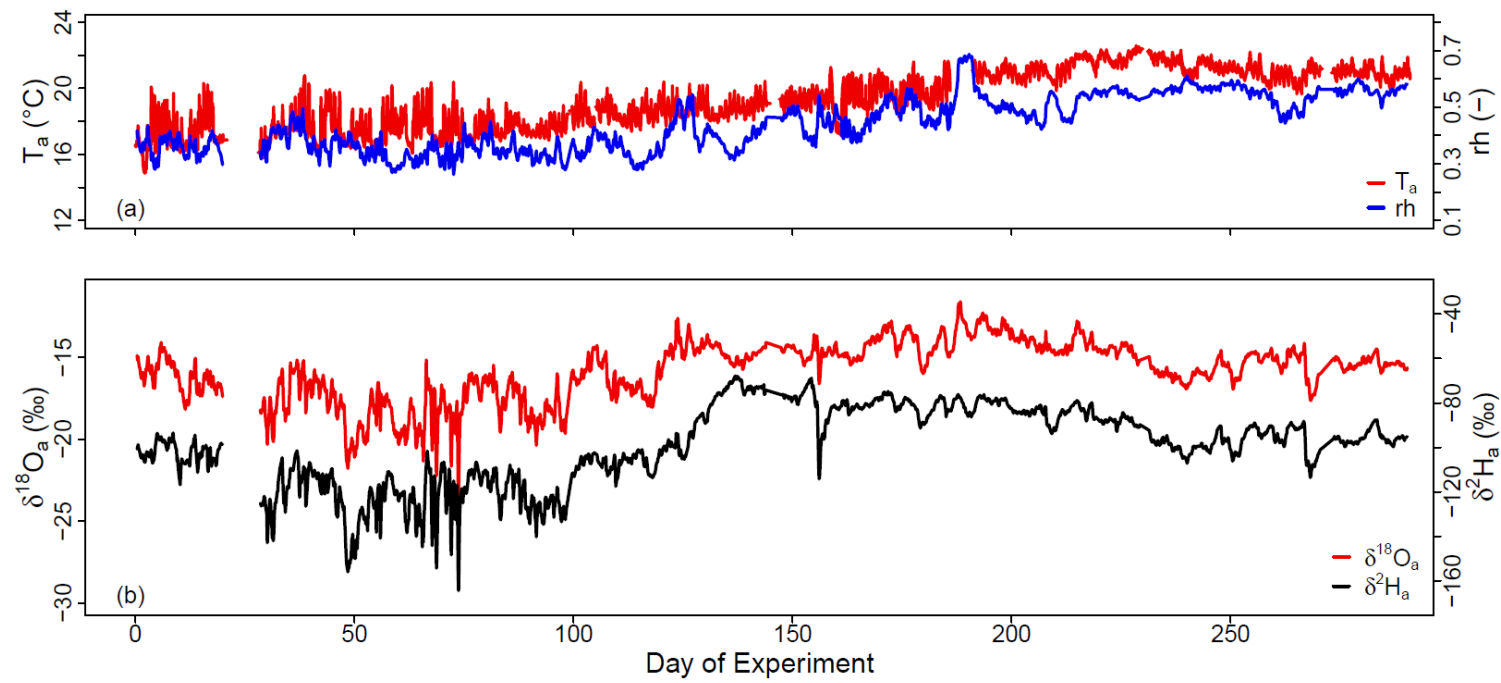
Figure 3. Time series of the laboratory ambient air temperature (T_a, in °C), relative humidity (rh, in %) and water vapor isotope compositions ($\delta^{18}O_a$ and δ^2H_a, in ‰ V-SMOW) over the course of the experiment
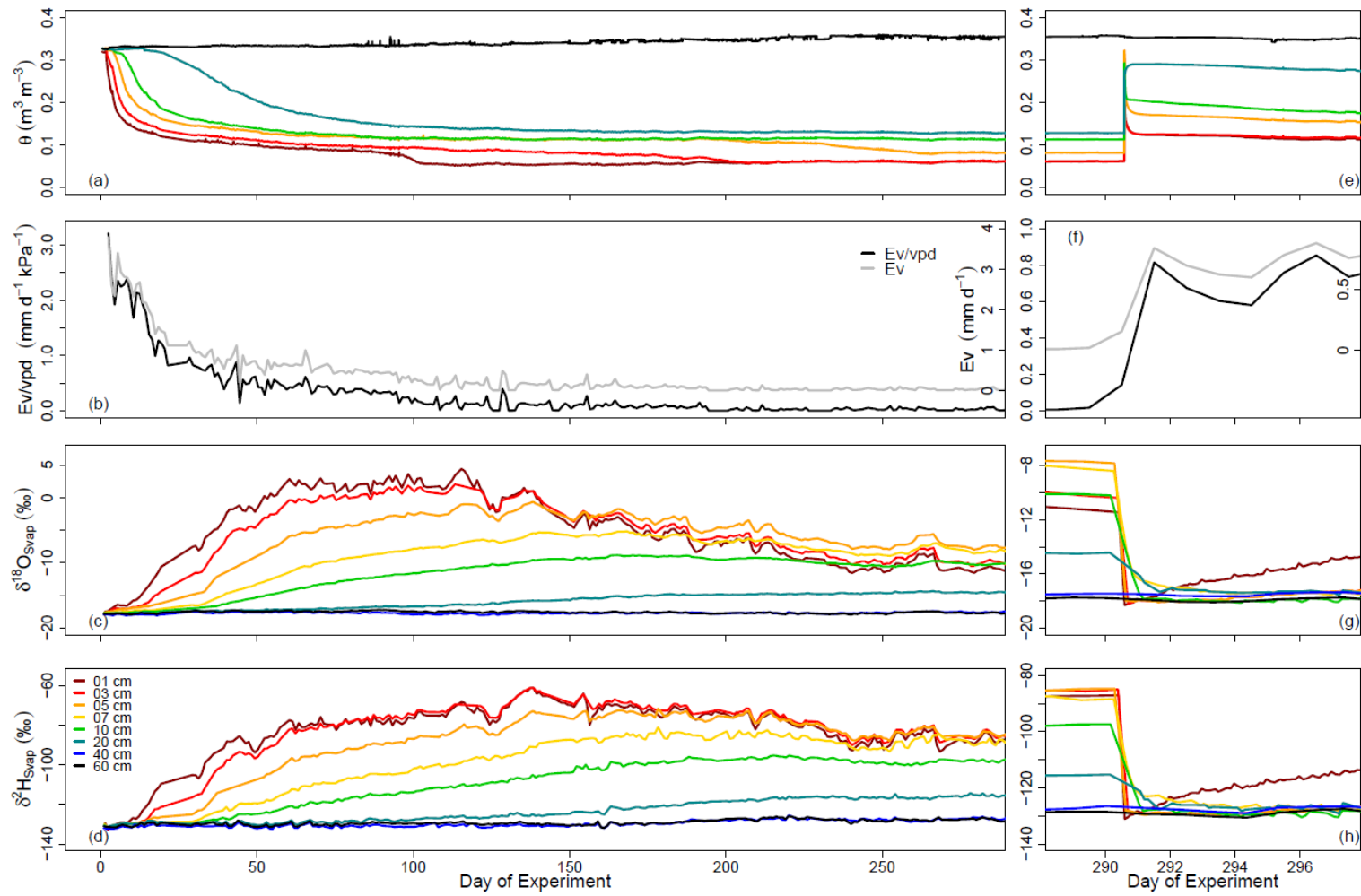
Figure 4. Time series of water content (θ, in $m^3\ m^{-3}$), evaporation flux (Ev, in $mm\ d^{-1}$), and water vapor isotope compositions ($\delta^{18}O_{Svap}$ and δ^2H_{Svap}, in ‰ V-SMOW) during the course of the experiment
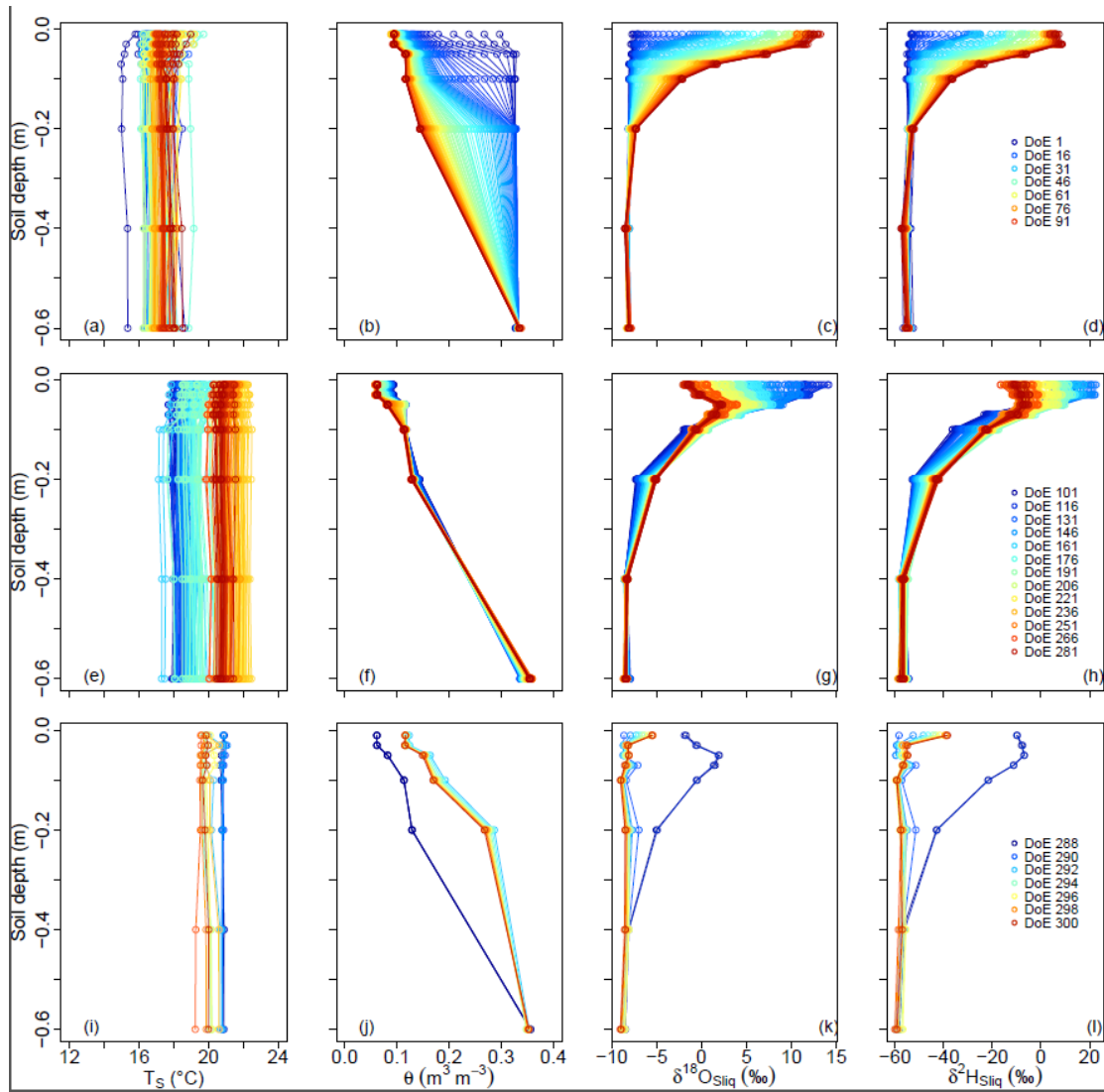
Figure 5. Soil temperature (T_S, in °C), water content (θ, in m^3 m^{-3}), and liquid water isotope compositions ($\delta^{18}O_{Sliq}$ and δ^2H_{Sliq}, in ‰ V-SMOW) profiles from Day of Experiment (DoE) 0 - 100 (top panel), from DoE 101 - 287 (middle panel), and from DoE 288 - 299 (bottom panel)
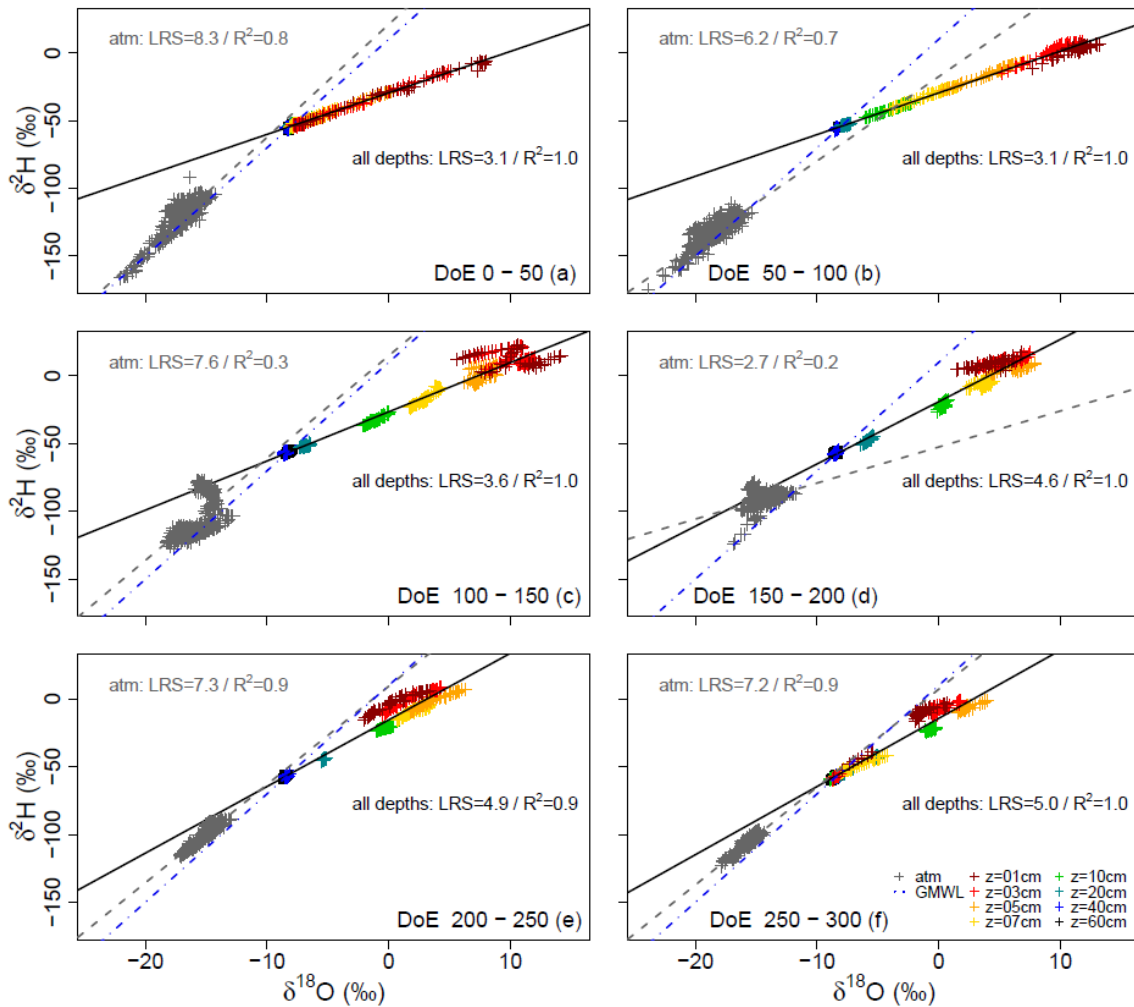
Figure 6. Linear regressions (gray dotted line) between laboratory atmosphere water vapor $\delta^{18}O$ and δ^2H (in ‰ V-SMOW) and between soil water $\delta^{18}O$ and δ^2H (solid black line). Each plot represents data from 50 consecutive days of experiment (DoE). Global Meteoric Water Line (GMWL, define by $\delta^2H = 8*\delta^{18}O + 10$, in blue dotted line) is shown on each sub-plot for comparison. Coefficient of determination (R^2) as well as the slope of the linear regressions (LRS) are reported
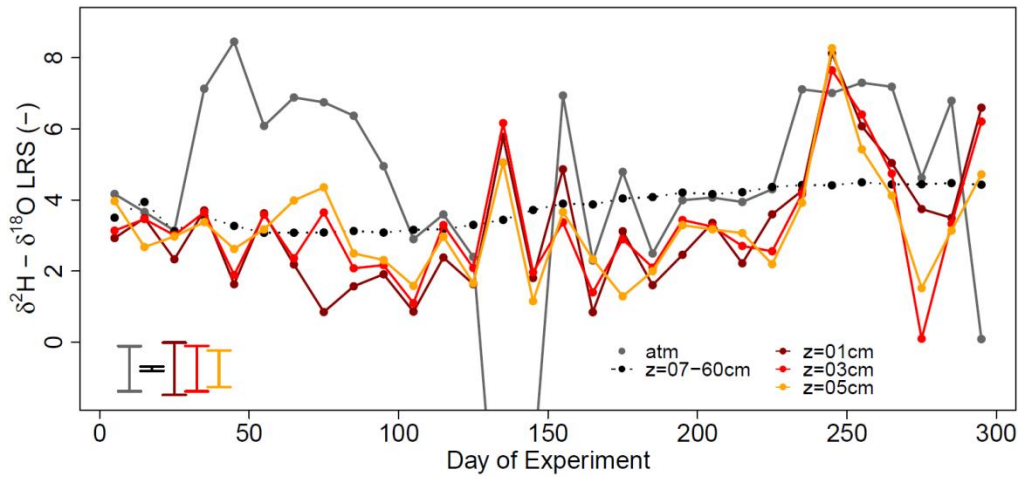
Figure 7. Time course of the slopes of the δ^{18}O-δ^2H linear regressions (LRS) for time intervals of ten consecutive days of atmosphere data (gray solid line), soil data from the upper three layers (01, 03, and 05 cm, colored solid lines), and combined soil data from the remaining bottom layers (from 07 to 60 cm, black dotted line). Mean standard errors are represented by the error bars in the bottom left corner
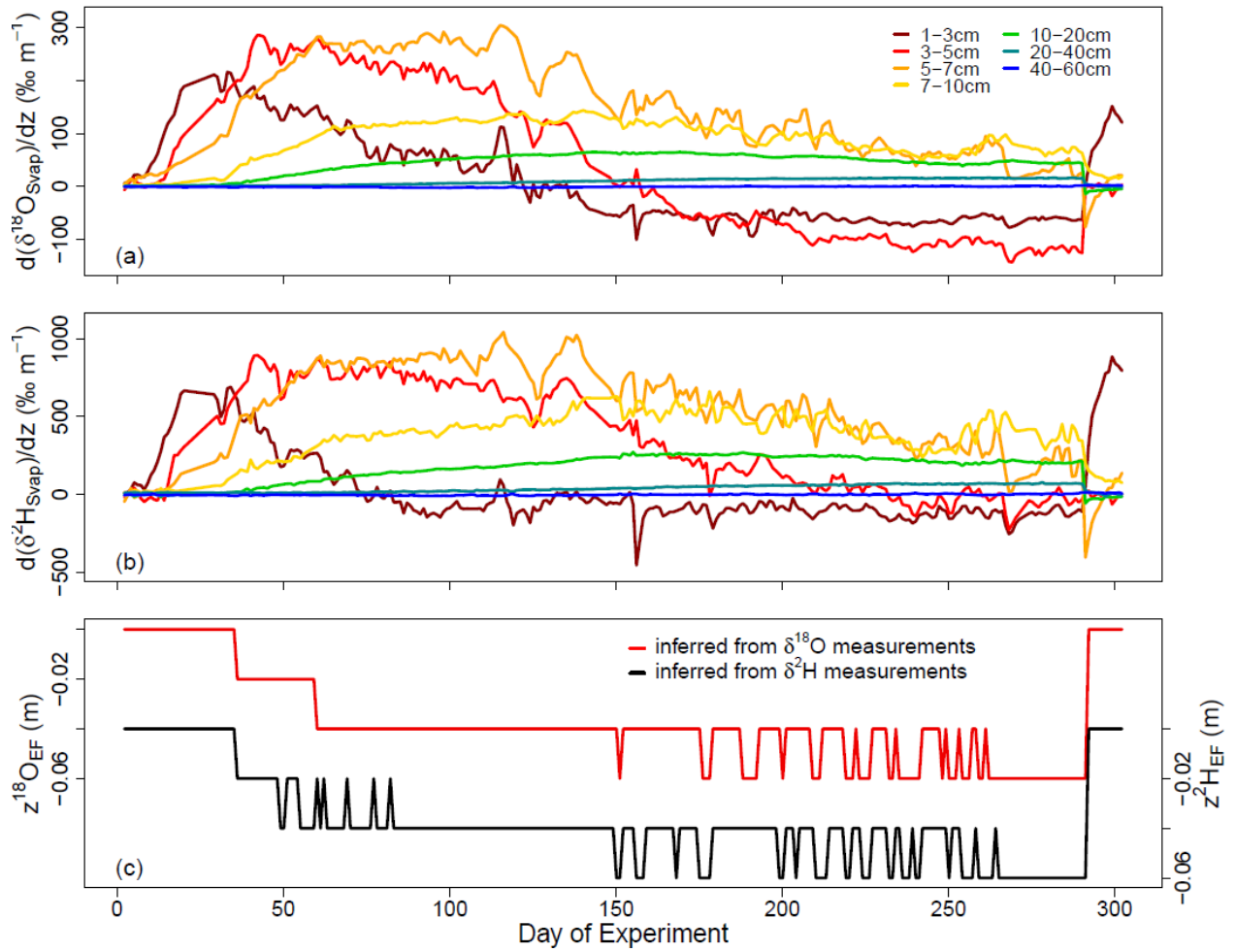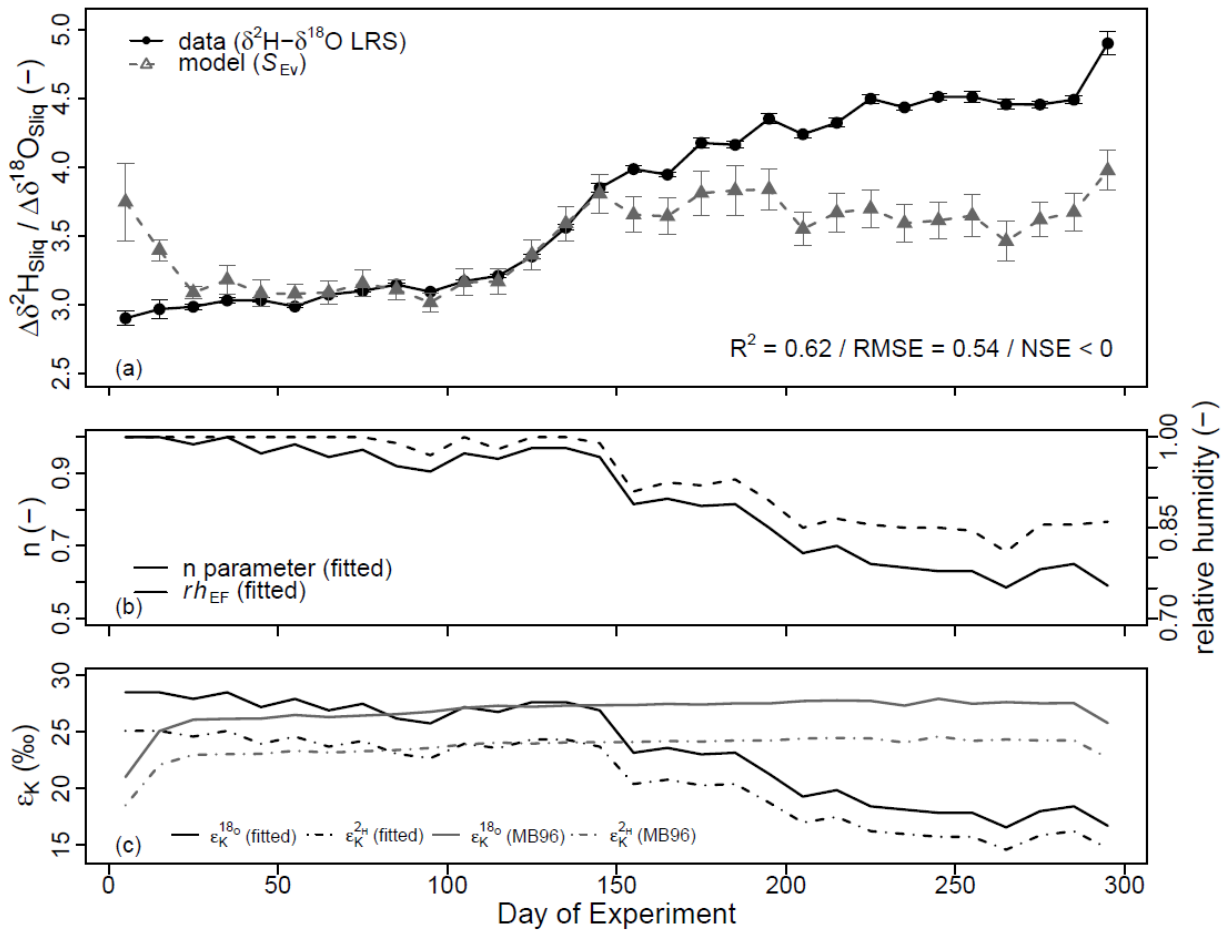
Figure 8. (a) and (b) $^1H^2H^{16}O$ and $^1H_2^{18}O$ composition gradients calculated between consecutive observation points in the soil. (c) Evolution of the evaporation front depths $z^{18}O_{EF}$ (red solid line) and z^2H_{EF} (black solid line) inferred from the $^1H^2H^{16}O$ and $^1H_2^{18}O$ composition gradients

Figure 9. (a) Comparison between soil liquid water $\delta^{18}O$-δ^2H linear regressions slopes (LRS, solid black line) calculated for time intervals of ten consecutive days and simulated time series of evaporation line slope (S_{Ev}, dotted gray line) obtained from Equations (3-6) (Gat et al., 1971, Merlivat, 1978, Mathieu and Bariac, 1996). Black error bars give the standard errors of the estimated $\delta^{18}O$-δ^2H LRS. Gray error bars are the standard errors associated with calculation of S_{Ev} following Phillips and Gregg (2001). Coefficient of determination (R^2), Root Mean Square Error (RMSE) and Nash and Sutcliffe Efficiency (NSE) between model and data are reported. (b) Time series of n parameter (Eq. (6)) and soil relative humidity at the Evaporation Front (rh_{EF}) that provided the best model-to-data fit. (c) ε_K^{2H} and ε_K^{18O} time series obtained from fitted n values ("fitted") and calculated following Mathieu and Bariac (1996) ("MB96")